The Comprehensive Response of the Magnetopause to the Impact of an Isolated Magnetosheath High-Speed Jet

Jiuqi Ma[1] , Binbin Tang[2] , Xinliang Gao[1,3] , Wenya Li[2] , Quanming Lu[1,3,4] , Wenlong Guo[5] , Jin Guo[1] , Huijie Liu[2] , and Chi Wang[2]

[1]CAS Key Laboratory of Geospace Environment, School of Earth and Space Sciences, University of Science and Technology of China, Hefei, China, [2]State Key Laboratory of Space Weather, National Space Science Center, Chinese Academy of Sciences, Beijing, China, [3]Collaborative Innovation Center of Astronautical Science and Technology, Harbin, China, [4]Deep Space Exploration Laboratory, CAS Center for Excellence in Comparative Planetology, Hefei, China, [5]Shandong Provincial Key Laboratory of Optical Astronomy and Solar-Terrestrial Environment, Institute of Space Sciences, Shandong University, Weihai, China

Abstract The magnetopause is the boundary between the Earth's magnetosphere and the solar wind. Magnetosheath high-speed jets can impact the magnetopause, causing local indentation and subsequently rebound. However, the comprehensive response of the magnetopause to the impact of a high-speed jet remains unclear. In this study, we establish that the full spatiotemporal response pattern of the magnetopause to the impact of an isolated magnetosheath high-speed jet can be characterized as an "Indentation-Rebounce-Relaxation" sequence from a statistical view. Based on the pressure balance, we estimate the spatial and temporal scales of the entire response process to range from 0.5 to 3.2 Earth radii and 0.9–4.7 min, respectively. Furthermore, we find that the interaction between the magnetopause and the high-speed jet during the rebounce phase distorts the magnetopause, subsequently generating pairs of field-aligned currents. These generated field-aligned currents may flow to the ionosphere, potentially contributing to magnetosphere-ionosphere coupling.

Plain Language Summary The Earth's magnetopause, separating the Earth's magnetosphere from the solar wind, is usually distorted by upstream magnetosheath pressure perturbations. One of these is the magnetosheath high-speed jets, which are localized dynamic pressure enhancements that can induce the local deformation of the magnetopause. Previous studies have found that magnetosheath high-speed jets can interact with the magnetopause, causing local indentation and subsequent rebound. However, due to the limitations of in-situ spacecraft observations, the complete response of the magnetopause to the impact of a high-speed jet remains unknown. Using Magnetospheric Multiscale satellite data, we establish a comprehensive response pattern of the magnetopause to an HSJ for the first time based on the statistical analysis of multiple cases, which is described as a sequence of "Indentation-Rebounce-Relaxation". This study will help us better understand the solar wind-magnetosphere coupling process.

1. Introduction

The magnetopause, which serves as the boundary separating the Earth's magnetosphere from the solar wind, plays a crucial role in the transfer of mass, momentum, and energy between the interplanetary environment and the magnetosphere. Its shape and location are influenced by conditions in the upstream solar wind dynamic pressure and the interplanetary magnetic field (Fairfield, 1971). Over the decades, numerous models of magnetopause have been developed, and the discrepancies between the model-predicted positions of the magnetopause and in-situ magnetopause crossings are usually small (Lin et al., 2010; Liu et al., 2015; Shue et al., 1997, 1998; Staples et al., 2020; Šafránková et al., 2002). However, there are situations where the observed magnetopause locations significantly diverge from model predictions (Grimmich et al., 2023; Xu et al., 2022). These prediction uncertainties can be caused by magnetosheath high-speed jets (HSJs), which can induce local deformations of the magnetopause, resulting in substantial deviations (Guo et al., 2024; Němeček et al., 2023; Shue et al., 2009; Wang et al., 2023).

HSJs are dynamic pressure enhancements in the magnetosheath plasma. The dynamic pressure enhancement results from the increases in plasma velocity, density, or both (Plaschke et al., 2018). The HSJs are common structures as they can appear many times per hour (Plaschke et al., 2013, 2016). Their sizes are around $0.1-1\ R_E$ (where R_E is the radius of Earth) (Guo et al., 2022; Plaschke et al., 2020; Ren et al., 2024). Many studies have
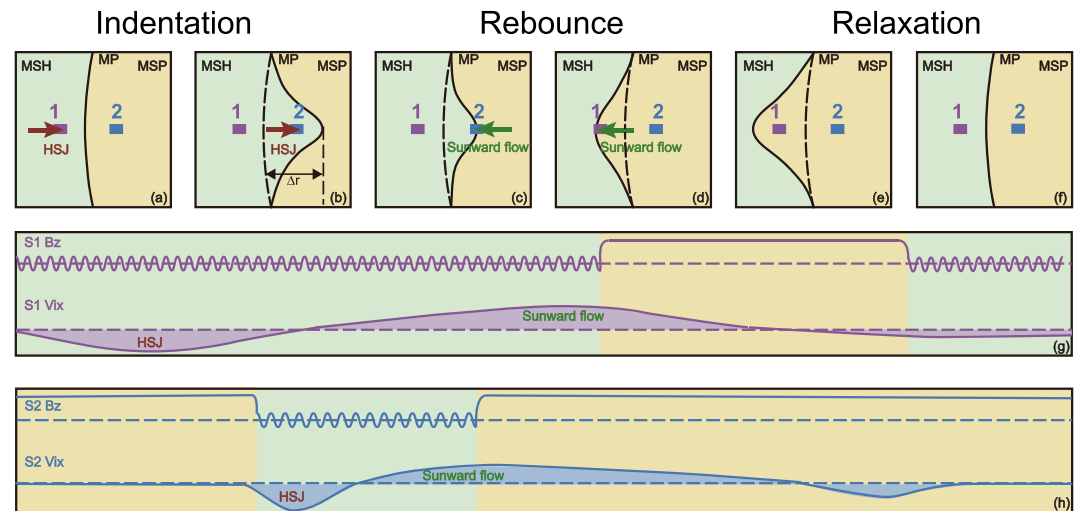
Figure 1. Schematic diagram illustrating the magnetopause's response to the HSJ. Panels (a–f) display the time sequence of the magnetopause's response to an isolated HSJ. The red arrows represent the HSJ, while the green arrows denote the sunward flow. The solid black line depicts the magnetopause, and the black dashed line shows the initial position of the magnetopause. Purple and blue rectangles mark the satellite positions in the two situations. Δr denotes the deepest indentation distance of the magnetopause. Panels (g–f) illustrate the temporal evolution of the z component of the magnetic field and the x component of the ion velocity for the two situations. The magnetosheath and magnetosphere environments are featured by light green and light yellow backgrounds, respectively.

shown that HSJs mostly occur in the magnetosheath downstream of the quasi-parallel bow shock (Archer & Horbury, 2013; Plaschke et al., 2013; Vuorinen et al., 2019). Thus, these results imply that the generation of HSJs can be linked to the quasi-parallel shock and the foreshock. The formation of HSJs can be related to the ripples on the bow shock (Hao et al., 2016; Hietala et al., 2009). Additionally, HSJs may result from the interaction between foreshock fluctuations and the bow shock (Karlsson et al., 2015; Raptis et al., 2022; Ren et al., 2023). Some HSJs can also be generated by the shock interaction with rotational discontinuities (Archer et al., 2012). The HSJs can indent the magnetopause (Amata et al., 2011; Dmitriev & Suvorova, 2012; Hietala et al., 2012; Shue et al., 2009), excite magnetopause eigenmodes (Archer et al., 2019), accelerate electrons (Liu et al., 2019), trigger magnetic reconnection (Hietala et al., 2018), and even be associated with auroral brightening (Han et al., 2017; Wang et al., 2018).

Recent studies have suggested that the magnetosheath HSJs can interact with the magnetopause, causing it to compress and subsequently rebound (Amata et al., 2011; Archer et al., 2012; Dmitriev & Suvorova, 2012; Plaschke et al., 2018). Shue et al. (2009) observed significant sunward plasma flows following the earthward movement of HSJs. They concluded that the jet induces a dent at the magnetopause, and subsequently magnetopause rebounds. Němeček et al. (2023) analyzed events where the magnetopause was observed several R_E farther from Earth than models had predicted. They revealed that the extremely distant locations of the magnetopause are caused by strong sunward flows, potentially originating from HSJs. These studies indicate that the magnetopause dents upon impact with HSJs and subsequently rebounds. However, it is still unclear whether the 'Indentation -Rebounce' pattern fully describes the response of the magnetopause to the HSJs. Based on these single-event studies, we infer the comprehensive response pattern of the magnetopause to an HSJ can be described as a sequence of "Indentation-Rebounce-Relaxation" (Figure 1). Utilizing observations from the Magnetospheric Multiscale (MMS) mission (Burch et al., 2016), the present study is performed to confirm this scenario from a statistical view. We select events when MMS is initially located on the magnetospheric and magnetosheath side respectively to capture the full response of the magnetopause to a magnetosheath HSJ. Meanwhile, we present the characteristic perturbations of field-aligned currents during the magnetopause response processes.

2. Data and Method

In this study, we investigate the magnetopause response to an isolated magnetosheath high-speed jet using data from MMS (Burch et al., 2016). For magnetic field measurements, we employed data from the fluxgate

magnetometer (FGM) (Russell et al., 2016), and particle data were acquired from the fast plasma investigation (FPI) (Pollock et al., 2016). The small distance between the four MMS spacecraft makes the observations from the four satellites similar, which allows us to primarily present the data from MMS1. The upstream solar wind parameters were obtained from the OMNI data set at a resolution of 1 min. The magnetopause location model used in this study is from Shue et al. (1998). All measurements used in this study are presented in Geocentric Solar Magnetospheric (GSM) coordinates.

Based on the MMS magnetopause crossing data set of 1,117 intervals from 2015 to 2018 (Haaland et al., 2020), we first selected magnetopause crossing possibly related to HSJs and determined the jets based on the solar wind dynamic pressure and the local background dynamic pressure (Plaschke et al., 2013; Raptis et al., 2020). We required the maximum x component of the magnetosheath dynamic pressure ($P_{d,MSH,x}$) to exceed half the solar wind dynamic pressure ($P_{d,sw}$). We also required the $P_{d,MSH,x}$ to be at least 1.5 times larger than the background average value. Then, the magnetosheath HSJ intervals were determined as the period where $P_{d,MSH,x} > 0.25\,P_{d,sw}$. Finally, we identified 163 magnetosheath HSJ intervals.

The response of the magnetopause to an HSJ can be described as a sequence of "Indentation-Rebounce-Relaxation" (Figure 1). To confirm the magnetopause rebound phase, we required a significant sunward flow (the x component of the ion velocity to be greater than +100 km/s) following the magnetosheath HSJs. 15 events satisfied this condition. Additionally, we included 5 response events from Guo et al. (2024) magnetopause crossing list, culminating in a total of 20 magnetopause response events (Table 1). Based on the initial position of MMS, we analyzed the 20 magnetopause response events falling into two situations: in Situation 1 (S1), the satellite was situated in the magnetosheath before detecting the magnetosheath HSJ; in Situation 2 (S2), the satellite was initially located in the magnetosphere. There were 11 events of S1 and 9 events of S2, respectively. As we focus on isolated (one-time pulse) high-speed jet events in this study, the situation when a jet or a high-pressure pulse continuously exists and disturbs the magnetopause with a convective discontinuity (Sibeck et al., 1999) should be excluded. For this purpose, we further confirm there is no discontinuity in the upstream solar wind based on criteria from Tsurutani and Smith (1979) and ensure that the normal direction of the magnetopause at the two crossings varies by less than 90°. By applying these constraints, additional 6 events are excluded from Table 1, leaving 8 events in S1 and 6 events in S2.

3. Results

For S1 events, the satellite (purple rectangle) is initially in the magnetosheath (Figure 1a), characterized by the typical magnetosheath magnetic field and plasmas (Figure 1g). The satellite subsequently detects a magnetosheath HSJ (red arrow, Figure 1a), featured by an increase in earthward plasma velocity (Figure 1g). When the magnetosheath HSJ hits the magnetopause, it causes the magnetopause (black line) to move inward (Figure 1b). After that, the magnetopause rebounds and moves sunward (Figure 1c). Then the satellite detects a sunward flow and enters the magnetosphere (Figure 1d). Finally, the magnetopause relaxes and moves to its original equilibrium position, allowing the satellite to return to the magnetosheath again (Figure 1f).

Figure 2 shows the MMS observations of an S1 magnetopause response event on 26 December 2016. Initially, MMS was located in the magnetosheath, as evidenced by the highly perturbed magnetic field, high ion density, and ion energies of ∼1 keV (Figures 2a, 2b and 2f–2g). MMS observed a significant increase in earthward dynamic pressure at 13:21:20 UT, identified as a magnetosheath HSJ (red-shaded interval). The maximum earthward dynamic pressure is around 3 nPa, which can cause a significant indentation of the magnetopause. At 13:23:30 UT, MMS detected a magnetopause crossing, accompanied by an obvious sunward flow. Subsequently, MMS entered the magnetosphere, where the magnetic field and ion density are more stabilized. These observations indicate that after the impact of a high-speed jet, the magnetopause rebounded and moved sunward. We utilized the MMS four-spacecraft timing method analysis of burst-mode magnetic field to estimate the velocity of the magnetopause (Harvey, C. C. 1998). The magnetopause moved sunward at 13:23:30 UT at a velocity of $104 \times [0.69, 0.72, 0.09]$ km/s. For convincing, we obtained the normal direction ([0.67, 0.73, 0.14]) based on the minimum variance analysis (MVA) on the burst-mode magnetic field (Sonnerup and Scheible 1998). The difference in the magnetopause normal directions calculated from the two methods is 4°. To ensure the reliability of the normal direction, we require the difference between the estimated normal directions by the two methods to be less than 15°. About 1 minute later, MMS detected another magnetopause crossing. Using the timing method, the

Table 1
Detailed Information on All Response Events

Event	Time (UT)	Normal (Shue98)	V_{MP} (timing, km/s)	Normal (timing)	Normal (MVA)	Δ r (Re)	$T_{model,l}$ (s)	T_{obs} (s)	Magnetic reconnection	θ_{B1B2} (°)
S1										
1	20151111/ 12:26:09.96	[0.94 0.28 −0.19]	216	[0.40 0.90 −0.19]	[0.40 0.88 −0.25]	1.61	191.96	138.02	yes	76
2	20161215/ 09:14:52.50	[0.99 0.14 0.00]	165	[0.66 0.46 −0.60]	[0.55 0.31 −0.78]	1.18	161.33	98.01	unclear	63
3	20161223/ 06:05:40.07	[1.00 −0.03 0.01]	86.2	[0.88 −0.15 −0.46]	[0.82 −0.40 −0.42]	3.18	287.21	215.83	unclear	37
4	20161226/ 12:47:04.52	[0.98 0.17 0.07]	146	[0.85 0.43 −0.31]	[0.93 0.28 −0.24]	1.50	136.41	132.90	no	37
5	20161226/ 13:23:11.21	[0.98 0.19 0.08]	104	[0.69 0.72 0.09]	[0.67 0.73 0.14]	1.40	153.25	101.91	no	54
6	20170108/ 12:20:00.05	[0.99 0.05 0.11]	83.2	[0.99 −0.12 0.09]	[0.97 −0.25 −0.02]	2.03	209.16	210.07	no	21
7	20170120/ 09:09:03.04	[0.98 −0.16 0.10]	187	[0.72 −0.69 −0.07]	[0.68 −0.74 −0.03]	1.28	144.61	132.23	yes	46
8	20190125/ 04:22:23.03	[0.91 −0.36 0.20]			[0.09 −0.98 0.15]	1.49	101.90	71.70	unclear	68
S2										
1	20151207/ 01:21:47.21	[0.97 −0.23 −0.06]	147	[0.89 −0.35 −0.28]	[0.87 −0.45 −0.20]	3.10	143.58	164.34	no	43
2	20151207/ 23:59:40.89	[0.96 −0.28 −0.06]	84.2	[0.27 −0.88 −0.39]	[0.21 −0.87 −0.45]	1.14	68.08	111.05	yes	67
3	20161226/ 11:22:19.20	[0.99 0.12 0.06]	284	[0.42 −0.87 −0.26]	[0.41 −0.86 −0.32]	1.64	58.30	104.18	no	29
4	20170110/ 04:11:25.57	[0.97 −0.23 −0.02]	82.2	[0.52 −0.62 −0.58]	[0.62 −0.53 −0.57]	1.55	109.69	215.41	unclear	84
5	20170204/ 06:28:25.88	[0.93 −0.36 0.02]	174	[0.13 0.93 0.34]	[0.04 0.97 0.24]	1.43	55.86	52.95	no	89
6	20161114/ 12:36:03.06	[0.89 0.43 −0.18]	73.1	[0.89 0.34 −0.31]	[0.97 0.19 −0.13]	0.52	68.90	136.60	unclear	24

magnetopause moved earthward at 13:24:30 UT at a velocity of −104 × [0.95, −0.30, 0.01] km/s. Accordingly, MMS returned to the magnetosheath, indicating that the magnetopause had undergone a relaxation phase.

The "Indentation" phase of the magnetopause cannot be directly observed in S1 events. Therefore, we present S2 events to demonstrate the process of magnetopause indentation following the impact of an HSJ. For S2 events, the satellite (blue rectangle) is initially located in the magnetosphere (Figure 1a), which is distinguished by a stable magnetic field (Figure 1g). When the satellite observes the magnetosheath HSJ (Figure 1h), the HSJ has already hit the magnetopause. The magnetopause moves earthward, causing the satellite to enter the magnetosheath (Figures 1b and 1h). Subsequently, the magnetopause rebounds and moves sunward (Figure 1c). Then the satellite observes the sunward flow and returns to the magnetosphere (Figures 1d and 1h). Finally, the magnetopause relaxes and returns to its original equilibrium position (Figures 1e and 1f).

Figure 3 presents a typical S2 magnetopause response event observed by MMS on 26 December 2016. MMS is initially located in the magnetosphere, characterized by a stable magnetic field and high energy (>10 keV) ions. MMS first crossed the magnetopause at 11:20:00 UT, and MMS entered the magnetosheath region. Immediately, MMS detected a magnetosheath high-speed jet, which is marked by a red-shaded region. The sharp change in the *y*-component of the magnetic field ahead of the HSJ (Figure 3a) may be related to the shock or the magnetic flux pileup generated by the high-speed jet (Hietala et al., 2009, 2012). Using the timing method, we estimated that the
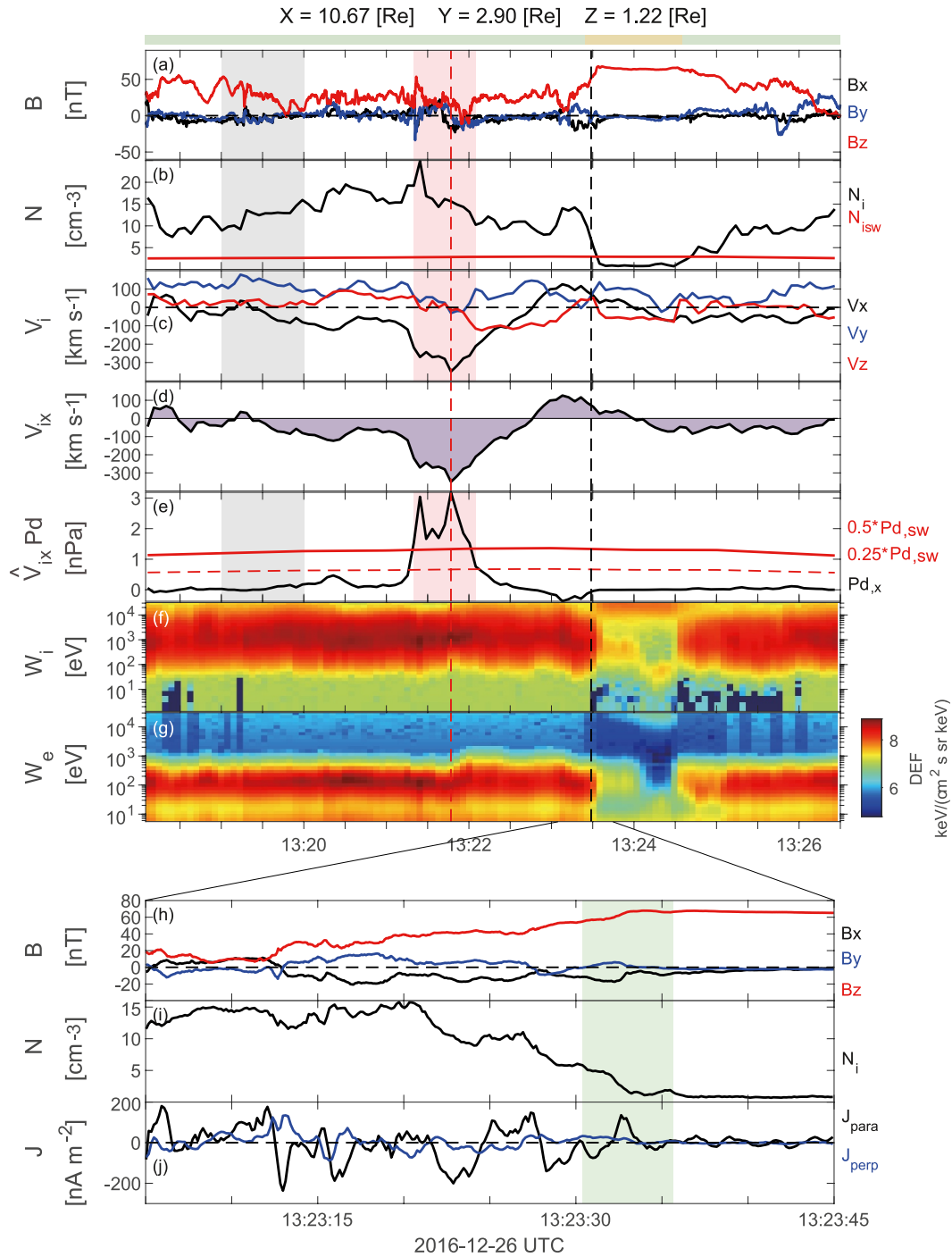
Figure 2. Overview of a typical S1 magnetopause response event observed by MMS on 12 December 2016. (a)–(g) displays the magnetic field, ion density, ion velocity, the *x* component of the ion velocity, earthward dynamic pressure, ion spectrogram, and electron spectrogram. (h)–(j) depicts the magnetic field, ion density, and the current of the burst-mode during the magnetopause crossing. The red solid line in panel (b) represents the solar wind density obtained from OMNI. In panel (e), the red solid and dashed lines indicate the solar wind dynamic pressure ($P_{d,sw}/2$, $P_{d,sw}/4$). The gray-shaded region in (a)–(g) highlights the background magnetosheath period. The red-shaded area marks the high-speed jet interval. The red dashed vertical line denotes the peak of the high-speed jet dynamic pressure, and the black dashed vertical line indicates the magnetopause crossing. The black and blue lines in panel (j) represent the presented parallel current and the perpendicular current component along the magnetopause, respectively. The green shaded region in panels (h)–(j) marks the magnetopause boundary layer at the magnetospheric side.

velocity of the magnetopause is $-271 \times [0.70, -0.63, -0.32]$ km/s. This demonstrates that the magnetopause was hit by the high-speed jet and moved earthward. Subsequently, MMS crossed the magnetopause again at 11:22:20 UT. MMS returned to the magnetosphere with an obvious sunward flow. This time, the velocity of magnetopause movement is $284 \times [0.42, -0.87, -0.26]$ km/s, suggesting the magnetopause was in a rebound phase. In most response events, the magnetopause rebounds only once, but there are also cases where the satellite crosses the magnetopause multiple times. We primarily focus on the first rebound process with the largest response scale. The subsequent magnetopause may oscillate and even further drive magnetopause surface waves, ultralow frequency waves (Archer et al., 2019; Plaschke, 2016), which we classify as part of the relaxation phase.

We further estimated the spatial and temporal response scales of the magnetopause to the impact of an isolated HSJ based on a simple pressure balance assumption. In this study, we considered the pressure balance between the total pressure in the magnetosheath (P_{MSH}, which includes thermal pressure, magnetic pressure, and dynamic pressure) and the magnetic pressure of the magnetosphere (P_{MSP}). Given that the magnetosphere's magnetic field is dipolar, the magnetic pressure of the magnetosphere is given by $P_{MSP} = \frac{B^2}{2\mu_0} = \frac{\lambda^2}{2\mu_0}\left(\frac{M_d}{r_0^3}\right)^2$, where B, μ_0, λ, M_d and r_0 represent the magnetic field, vacuum permeability, magnetospheric compressibility coefficient, magnetic dipole moment, and radial distance from the magnetopause to the Earth's center, respectively. Here, we roughly take λ as a constant. We assume that a change ΔP in the total pressure of the magnetosheath, causes the magnetopause to move a maximum distance of Δr (Figure 1b). The pressure balance is expressed as $P_{MSH} + \Delta P = \frac{\lambda^2}{2\mu_0}\left(\frac{M_d}{(r_0 - \Delta r)^3}\right)^2$, and the change in the total pressure of the magnetosheath ΔP can be written as $\Delta P = \frac{\lambda^2}{2\mu_0}\left(\frac{M_d}{(r_0 - \Delta r)^3}\right)^2 - \frac{\lambda^2}{2\mu_0}\left(\frac{M_d}{r_0^3}\right)^2$. By substituting P_{MSH} into the equation, we derive the correlation between ΔP and Δr:

$$\Delta P = P_{MSH}\left[\left(1 - \frac{\Delta r}{r_0}\right)^{-6} - 1\right] \tag{1}$$

Applying the first-order Taylor approximation, Equation 1 can be written as:

$$\frac{\Delta P}{P_{MSH}} \approx 6\frac{\Delta r}{r_0} \tag{2}$$

P_{MSH} corresponds to the average total pressure in the magnetosheath, such as the interval indicated by the gray-shaded region in Figure 2. ΔP is calculated from the enhancement of dynamic pressure along the normal direction provided by the model (Shue et al., 1998). Equation 2 shows how Δr changes linearly if ΔP is small. During the impact of an HSJ, $\Delta P/P_{MSH}$ can be significantly larger than 2, making Equation 2 not applicable. Consequently, we directly solve Equation 1 to obtain Δr. In the two events mentioned above, Δr is 1.4 R_E and 1.64 R_E, respectively. The estimated magnetopause indentation is constant with results from the fast cold ion motion inside the magnetopause, which has been used as an indicator of magnetopause deformation (Guo et al., 2024).

We define T_{model} as the modeled response time from the peak of the HSJ dynamic pressure observed by the satellite (t_1, red vertical dashed line in Figures 2 and 3) to the magnetopause observed by the satellite (t_2, black vertical dashed line in Figures 2 and 3). The response time can also be scaled using $T_{model} = X_{model}/V$, where X_{model} is twice the distance from the satellite to the deepest indentation of the magnetopause, and V represents the average speed during the impact process, which is roughly taken as the mean value of V_n (the velocity along the magnetopause normal direction) at times t_1 and t_2 here. This means that the magnetopause is assumed to move at a constant speed, and we further assume that the scale of the magnetopause indentation is comparable to that of the magnetopause rebound. Thus, the longest response time ($T_{model,1,l}$) can be inferred as $T_{model,1,l} = 4\Delta r/V$. Next, we estimate the shortest response times ($T_{model,1,s}$). This corresponds to the situation when the satellite is located just outside of the magnetopause. The magnetopause is compressed and then rebounds, moving a total distance of $2\Delta r$, resulting in $T_{model,1,s} = 2\Delta r/V$. For S2 events, the longest response time ($T_{model,2,l}$) corresponds to the situation when the satellite is located just inside of the magnetopause. The magnetopause is compressed and rebounded, moving a total distance of $2\Delta r$, so $T_{model,2,l} = 2\Delta r/V$. The shortest response times ($T_{model,2,s}$) correspond to the cases when the satellite is located at the deepest indentation point. The satellite observes the
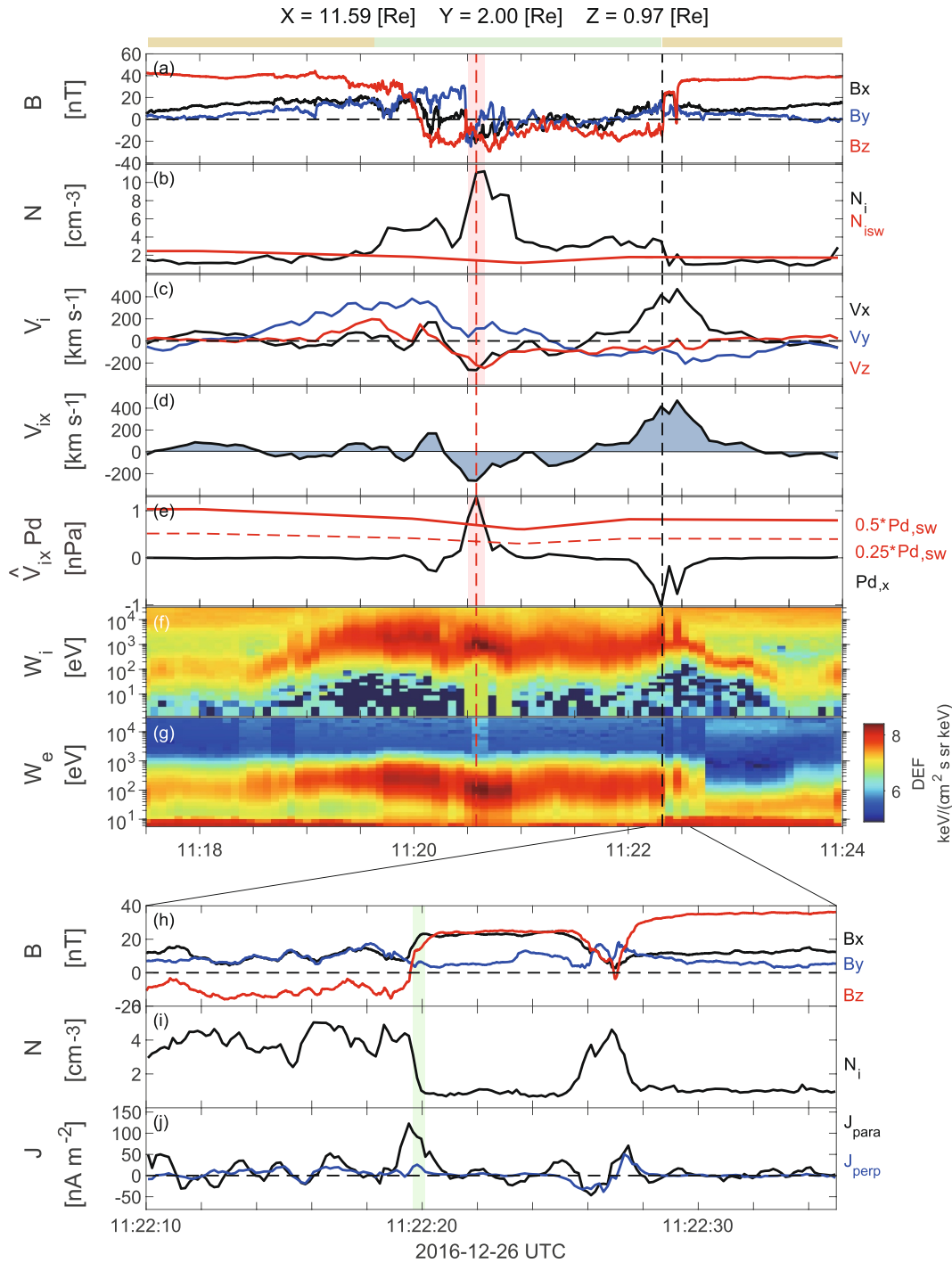
Figure 3. Overview of a typical S2 magnetopause response event on 12 December 2016. The figure format is similar to that in Figure 2.

sunward flow immediately after observing the HSJ, so the shortest response time should be zero. This method provides a quantitative assessment of whether an HSJ is directly responsible for the subsequent magnetopause crossing. The T_{model} of the above two cases are 76–154 s and 0–58 s, respectively. The response times in observations are 101 and 104 s, respectively. In all 14 events, we find the observed response time matches the model predictions in 8 events (7 S1 events and 1 S2 event, Table 1). This discrepancy can be attributed to the simple assumptions stated above, and a more detailed analysis should be performed in the future.
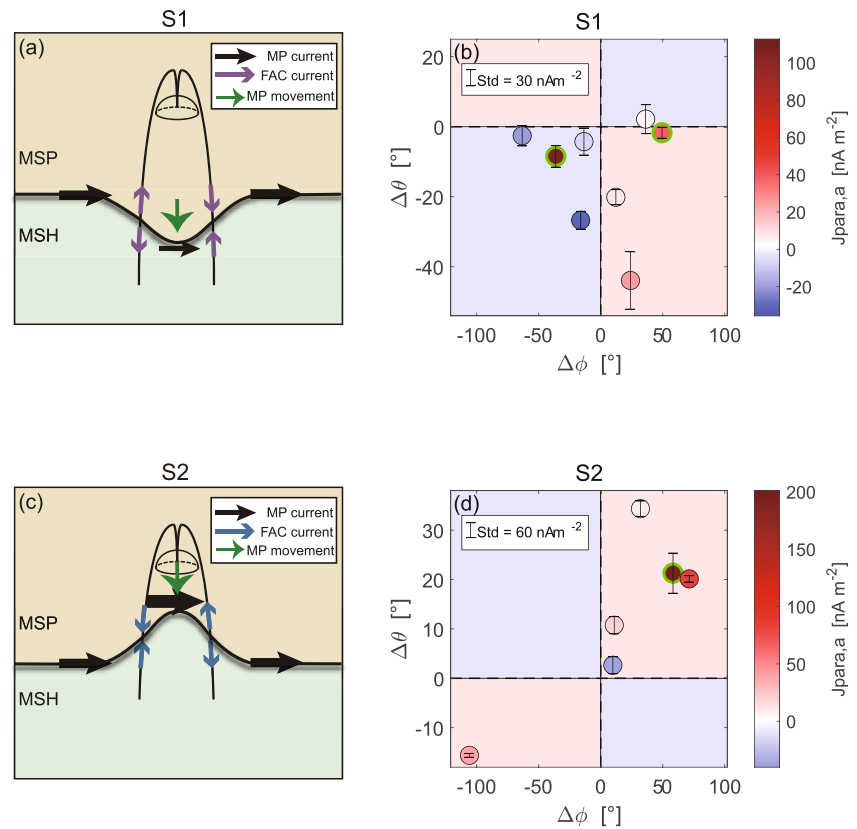
Figure 4. The distribution of field-aligned currents during the magnetopause rebounce phase. Panels (a) and (c) present schematic diagrams of the field-aligned current distribution for two situations. The black arrow indicates the magnetopause current, while the purple and blue arrows denote the field-aligned current pairs generated by the magnetopause deformation in the two situations. The green arrows indicate the sunward motion of the magnetopause. Light yellow and light green backgrounds separate the magnetosphere and magnetosheath environments. Panels (b) and (d) are the observations from multiple events. The $\Delta\theta$ and $\Delta\Phi$ represent the deviations between the normal of the magnetopause model and the actual magnetopause normal in the polar and azimuthal directions, respectively. $J_{para,a}$ is the average value of the field-aligned current in the magnetopause boundary layer at the magnetospheric side with standard deviations. The black vertical lines indicate error bars. The green outer circle denotes possible magnetic reconnection events as listed in Table 1. The four-colored sectors in panels (b) and (c) correspond to the direction of the field-aligned current shown in panels (a) and (c).

When an HSJ interacts with the magnetopause, the magnetopause becomes distorted, leading to changes in the magnetic field and resulting in perturbations of field-aligned currents. As shown in Figures 2h–2j and 3h-3j, when the satellite crosses from the magnetosheath to the magnetosphere, it detects obvious field-aligned currents. The current density is calculated by $J = qn (V_i - V_e)$, where n is the ion number density, V_i and V_e are the ion and electron velocities. Figure 4 shows the dependence of field-aligned currents during the different magnetopause deformation stages. For S1 events, the sunward magnetopause motion corresponds to the magnetopause rebound phase. When magnetopause moves sunward, the magnetic field magnitude weakens, further causing the magnetopause current (the black arrows in Figure 4a) to be reduced. Therefore, on the dawn side of the deformation region, the current will flow away for current continuity, producing a pair of upward/downward field-aligned currents (purple arrows). Similarly, on the dusk side of the deformation, the other pair of field-aligned currents are generated (purple arrows). For S2 events, the deformation also corresponds to the sunward motion of the magnetopause. As presented in Figure 4c, we can find two pairs of field-aligned currents (blue arrows) are similarly generated, but in different directions compared with Figure 4a. The direction of the field-aligned current pairs is consistent with Glassmeier and Heppner (1992), and our results further show that the pairs of field-aligned currents change directions during the magnetopause response to an HSJ.

Figures 4b and 4d show the statistical results of field-aligned current. $J_{para,a}$ denotes the average field-aligned current within the magnetopause boundary layer at the magnetospheric side (the green-shaded areas shown in

Figures 2j and 3j), which is calculated at the magnetopause crossings with sunward plasma flows. We compared the normal direction of the magnetopause obtained by the timing method (Table 1) with the normal direction of the magnetopause provided by the model (Shue et al., 1998). Based on the difference between the two normal directions, we can infer in which quadrant of the magnetopause deformation the satellite is located (divided into four sectors). The sign of $\Delta\theta$ indicates whether the satellite is located on the northern or southern side, and the sign of $\Delta\phi$ indicates whether the satellite is located on the dawn or dusk side of the deformation. In S1 events, the direction of the field-aligned current in six out of 8 events is consistent with predictions. In S2 events, the direction of the field-aligned current in five out of 6 events matches. This result shows that most of these events can generate significant field-aligned currents. The closure of these field-aligned currents is another interesting issue, which can close locally surrounding the deformed magnetopause region or connect to Earth. However, it is not conclusive from in-situ MMS observations, and the related investigation can be verified from auroral images, such as from the Solar wind Magnetosphere Ionosphere Link Explorer (SMILE) mission (Branduardi-Raymont et al., 2018; C. Wang and Branduardi-Raymond, 2018) and other observations. We noted that all other magnetopause activities (such as magnetic reconnection (Ma et al., 1995)), which can also generate strong field-aligned current, are ignored here due to the limited data set. In Figures 4a and 4d, three clearly identified reconnection events are marked with green circles, regardless of whether they are related to HSJs. These effects should be excluded if a larger data set is available.

4. Conclusions

In this study, we have demonstrated the full spatiotemporal response of the magnetopause to the impact of an isolated magnetosheath HSJ, manifested as a sequence of "Indentation-Rebounce-Relaxation". Based on the pressure balance assumption, we estimate the spatial and temporal scales of the entire response process to range from 0.5 to 3.2 Earth radii and 0.9–4.7 min, respectively. We also reveal that the interaction of the magnetopause with the HSJ leads to distortion of the magnetopause, subsequently generating pairs of field-aligned currents.

This study provides a comprehensive depiction of the magnetopause's response to the impact of an HSJ. The upcoming Solar wind Magnetosphere Ionosphere Link Explorer (SMILE) mission will offer new opportunities to investigate how the magnetopause responds to the solar wind by imaging the magnetopause with soft X-rays. By combining time series of magnetopause images with in situ observations, our understanding of the magnetopause response to HSJs will be significantly improved in the future.

Data Availability Statement

The MMS data are obtained from the MMS Science Data Center (https://lasp.colorado.edu/mms/sdc/public/about/browse-wrapper/), and the solar wind data are from the OMNI website (https://omniweb.gsfc.nasa.gov). The MP response events list can be found at J. Ma and Tang (2024).

References

Amata, E., Savin, S., Ambrosino, D., Bogdanova, Y., Marcucci, M., Romanov, S., & Skalsky, A. (2011). High kinetic energy density jets in the Earth's magnetosheath: A case study. *Planetary and Space Science*, *59*(7), 482–494. https://doi.org/10.1016/j.pss.2010.07.021

Archer, M., Hietala, H., Hartinger, M. D., Plaschke, F., & Angelopoulos, V. (2019). Direct observations of a surface eigenmode of the dayside magnetopause. *Nature Communications*, *10*(1), 615. https://doi.org/10.1038/s41467-018-08134-5

Archer, M., & Horbury, T. (2013). Magnetosheath dynamic pressure enhancements: Occurrence and typical properties. In *Paper presented at Ann Geophys-Germany*. Copernicus Publications Göttingen.

Archer, M., Horbury, T., & Eastwood, J. (2012). Magnetosheath pressure pulses: Generation downstream of the bow shock from solar wind discontinuities. *Journal of Geophysical Research*, *117*(A5), A05228. https://doi.org/10.1029/2011ja017468

Branduardi-Raymont, G., Wang, C., Escoubet, C., Adamovic, M., Agnolon, D., Berthomier, M., et al. (2018). SMILE Definition study report (red book). *ESA/SCI*, *2018*, 1.

Burch, J., Moore, T., Torbert, R., & Giles, B.-h. (2016). Magnetospheric multiscale overview and science objectives. *Space Science Reviews*, *199*(1–4), 5–21. https://doi.org/10.1007/s11214-015-0164-9

Dmitriev, A., & Suvorova, A. (2012). Traveling magnetopause distortion related to a large-scale magnetosheath plasma jet: THEMIS and ground-based observations. *Journal of Geophysical Research*, *117*(A8), A08217. https://doi.org/10.1029/2011ja016861

Fairfield, D. H. (1971). Average and unusual locations of the Earth's magnetopause and bow shock. *Journal of Geophysical Research*, *76*(28), 6700–6716. https://doi.org/10.1029/ja076i028p06700

Glassmeier, K.-H., & Heppner, C. (1992). Traveling magnetospheric convection twin vortices: Another case study, global characteristics, and a model. *Journal of Geophysical Research*, *97*(A4), 3977–3992. https://doi.org/10.1029/91ja02464

Grimmich, N., Plaschke, F., Archer, M. O., Heyner, D., Mieth, J. Z., Nakamura, R., & Sibeck, D. G. (2023). Study of extreme magnetopause distortions under varying solar wind conditions. *Journal of Geophysical Research: Space Physics*, *128*(8), e2023JA031603. https://doi.org/10.1029/2023ja031603

Guo, J., Lu, S., Lu, Q., Lin, Y., Wang, X., Ren, J., et al. (2022). Large-scale high-speed jets in Earth's magnetosheath: Global hybrid simulations. *Journal of Geophysical Research: Space Physics*, *127*(6), e2022JA030477. https://doi.org/10.1029/2022ja030477

Guo, W., Tang, B., Zhang, Q., Li, W., Yang, Z., Sun, T., et al. (2024). The magnetopause deformation indicated by fast cold ion motion. *Journal of Geophysical Research: Space Physics*, *129*(2), e2023JA032121. https://doi.org/10.1029/2023ja032121

Haaland, S., Paschmann, G., Øieroset, M., Phan, T., Hasegawa, H., Fuselier, S., et al. (2020). Characteristics of the flank magnetopause: MMS results. *Journal of Geophysical Research: Space Physics*, *125*(3), e2019JA027623. https://doi.org/10.1029/2019ja027623

Han, D. S., Hietala, H., Chen, X. C., Nishimura, Y., Lyons, L., Liu, J. J., et al. (2017). Observational properties of dayside throat aurora and implications on the possible generation mechanisms. *Journal of Geophysical Research: Space Physics*, *122*(2), 1853–1870. https://doi.org/10.1002/2016ja023394

Hao, Y., Lembège, B., Lu, Q., & Guo, F. (2016). Formation of downstream high-speed jets by a rippled nonstationary quasi-parallel shock: 2-D hybrid simulations. *Journal of Geophysical Research: Space Physics*, *121*(3), 2080–2094. https://doi.org/10.1002/2015ja021419

Harvey, C. C. (1998). Spatial gradients and the volumetric tensor. In G. Paschmann & P. Daly (Eds.), *Analysis methods for multi-spacecraft data* (pp. 307–322). ISSI/ESA.

Hietala, H., Laitinen, T. V., Andréeová, K., Vainio, R., Vaivads, A., Palmroth, M., et al. (2009). Supermagnetosonic jets behind a collisionless quasiparallel shock. *Physical Review Letters*, *103*(24), 245001. https://doi.org/10.1103/physrevlett.103.245001

Hietala, H., Partamies, N., Laitinen, T. V., Clausen, L. B. N., Facskó, G., Vaivads, A., et al. (2012). Supermagnetosonic subsolar magnetosheath jets and their effects: From the solar wind to the ionospheric convection. *Annals of Geophysics*, *30*(1), 33–48. https://doi.org/10.5194/angeo-30-33-2012

Hietala, H., Phan, T., Angelopoulos, V., Oieroset, M., Archer, M. O., Karlsson, T., & Plaschke, F. (2018). In situ observations of a magnetosheath high-speed jet triggering magnetopause reconnection. *Geophysical Research Letters*, *45*(4), 1732–1740. https://doi.org/10.1002/2017gl076525

Karlsson, T., Kullen, A., Liljeblad, E., Brenning, N., Nilsson, H., Gunell, H., & Hamrin, M. (2015). On the origin of magnetosheath plasmoids and their relation to magnetosheath jets. *Journal of Geophysical Research: Space Physics*, *120*(9), 7390–7403. https://doi.org/10.1002/2015ja021487

Lin, R., Zhang, X., Liu, S., Wang, Y., & Gong, J. (2010). A three-dimensional asymmetric magnetopause model. *Journal of Geophysical Research*, *115*(A4). https://doi.org/10.1029/2009ja014235

Liu, T. Z., Hietala, H., Angelopoulos, V., Omelchenko, Y., Roytershteyn, V., & Vainio, R. (2019). THEMIS observations of particle acceleration by a magnetosheath jet-driven bow wave. *Geophysical Research Letters*, *46*(14), 7929–7936. https://doi.org/10.1029/2019gl082614

Liu, Z. Q., Lu, J., Wang, C., Kabin, K., Zhao, J., Wang, M., et al. (2015). A three-dimensional high Mach number asymmetric magnetopause model from global MHD simulation. *Journal of Geophysical Research: Space Physics*, *120*(7), 5645–5666. https://doi.org/10.1002/2014ja020961

Ma, J., & Tang, B. (2024). Dataset for the paper "the comprehensive response of the magnetopause to the impact of a magnetosheath high-speed jet" [Dataset]. *Zenodo*. https://doi.org/10.5281/zenodo.12640419

Ma, Z., Lee, L., & Otto, A. (1995). Generation of field-aligned currents and Alfvén waves by 3D magnetic reconnection. *Geophysical Research Letters*, *22*(13), 1737–1740. https://doi.org/10.1029/95gl01430

Němeček, Z., Šafránková, J., Grygorov, K., Mokrý, A., Pi, G., Aghabozorgi Nafchi, M., et al. (2023). Extremely distant magnetopause locations caused by magnetosheath jets. *Geophysical Research Letters*, *50*(24), e2023GL106131. https://doi.org/10.1029/2023gl106131

Plaschke, F. (2016). ULF waves at the magnetopause. *Low-frequency waves in space plasmas*, 193–212. https://doi.org/10.1002/9781119055006.ch12

Plaschke, F., Hietala, H., & Angelopoulos, V. (2013). Anti-sunward high-speed jets in the subsolar magnetosheath. In *Paper presented at Ann Geophys-Germany*. Copernicus Publications Göttingen.

Plaschke, F., Hietala, H., Angelopoulos, V., & Nakamura, R. (2016). Geoeffective jets impacting the magnetopause are very common. *Journal of Geophysical Research: Space Physics*, *121*(4), 3240–3253. https://doi.org/10.1002/2016ja022534

Plaschke, F., Hietala, H., Archer, M., Blanco-Cano, X., Kajdič, P., Karlsson, T., et al. (2018). Jets downstream of collisionless shocks. *Space Science Reviews*, *214*(5), 1–77. https://doi.org/10.1007/s11214-018-0516-3

Plaschke, F., Hietala, H., & Vörös, Z. (2020). Scale sizes of magnetosheath jets. *Journal of Geophysical Research: Space Physics*, *125*(9), e2020JA027962. https://doi.org/10.1029/2020ja027962

Pollock, C., Moore, T., Jacques, A., Burch, J., Gliese, U., Saito, Y., et al. (2016). Fast plasma investigation for magnetospheric multiscale. *Space Science Reviews*, *199*(1–4), 331–406. https://doi.org/10.1007/s11214-016-0245-4

Raptis, S., Karlsson, T., Plaschke, F., Kullen, A., & Lindqvist, P. A. (2020). Classifying magnetosheath jets using MMS: Statistical properties. *Journal of Geophysical Research: Space Physics*, *125*(11), e2019JA027754. https://doi.org/10.1029/2019ja027754

Raptis, S., Karlsson, T., Vaivads, A., Pollock, C., Plaschke, F., Johlander, A., et al. (2022). Downstream high-speed plasma jet generation as a direct consequence of shock reformation. *Nature Communications*, *13*(1), 598. https://doi.org/10.1038/s41467-022-28110-4

Ren, J., Guo, J., Lu, Q., Lu, S., Gao, X., Ma, J., & Wang, R. (2024). Honeycomb-like magnetosheath structure formed by jets: Three-dimensional global hybrid simulations. *Geophysical Research Letters*, *51*(12), e2024GL109925. https://doi.org/10.1029/2024gl109925

Ren, J., Lu, Q., Guo, J., Gao, X., Lu, S., Wang, S., & Wang, R. (2023). Two-dimensional hybrid simulations of high-speed jets downstream of quasi-parallel shocks. *Journal of Geophysical Research: Space Physics*, *128*(8), e2023JA031699. https://doi.org/10.1029/2023ja031699

Russell, C., Anderson, B., Baumjohann, W., Bromund, K., Dearborn, D., Fischer, D., et al. (2016). The magnetospheric multiscale magnetometers. *Space Science Reviews*, *199*, 189–256. https://doi.org/10.1007/978-94-024-0861-4_8

Šafránková, J., Němeček, Z., Dušík, Š., Přech, L., Sibeck, D., & Borodkova, N. (2002). The magnetopause shape and location: A comparison of the interball and Geotail observations with models. In *Paper presented at Ann Geophys-Germany*. Copernicus GmbH.

Shue, J. H., Chao, J., Fu, H., Russell, C., Song, P., Khurana, K., & Singer, H. (1997). A new functional form to study the solar wind control of the magnetopause size and shape. *Journal of Geophysical Research*, *102*(A5), 9497–9511. https://doi.org/10.1029/97ja00196

Shue, J. H., Chao, J. K., Song, P., McFadden, J., Suvorova, A., Angelopoulos, V., et al. (2009). Anomalous magnetosheath flows and distorted subsolar magnetopause for radial interplanetary magnetic fields. *Geophysical Research Letters*, *36*(18), L18112. https://doi.org/10.1029/2009gl039842

Shue, J. H., Song, P., Russell, C., Steinberg, J., Chao, J., Zastenker, G., et al. (1998). Magnetopause location under extreme solar wind conditions. *Journal of Geophysical Research*, *103*(A8), 17691–17700. https://doi.org/10.1029/98ja01103

Sibeck, D. G., Borodkova, N. L., Schwartz, S. J., Owen, C. J., Kessel, R., Kokubun, S., et al. (1999). Comprehensive study of the magnetospheric response to a hot flow anomaly. *Journal of Geophysical Research*, *104*(A3), 4577–4593.

Sonnerup, B. U. Ö., & Scheible, M. (1999). Minimum and maximum variance analysis, in *Analysis methods for multi-spacecraft data*. ESA, (Eds) G. Paschmann, & P. Daly (pp. 185–220).

Staples, F., Rae, I., Forsyth, C., Smith, A., Murphy, K., Raymer, K., et al. (2020). Do statistical models capture the dynamics of the magnetopause during sudden magnetospheric compressions? *Journal of Geophysical Research: Space Physics*, *125*(4), e2019JA027289. https://doi.org/10.1029/2019ja027289

Tsurutani, B. T., & Smith, E. J. (1979). Interplanetary discontinuities: Temporal variations and the radial gradient from 1 to 8.5 AU. *Journal of Geophysical Research*, *84*(A6), 2773–2787. https://doi.org/10.1029/ja084ia06p02773

Vuorinen, L., Hietala, H., & Plaschke, F. (2019). Jets in the magnetosheath: IMF control of where they occur. In *Paper presented at Ann Geophys-Germany*. Copernicus Publications Göttingen.

Wang, B., Nishimura, Y., Hietala, H., Lyons, L., Angelopoulos, V., Plaschke, F., et al. (2018). Impacts of magnetosheath high-speed jets on the magnetosphere and ionosphere measured by optical imaging and satellite observations. *Journal of Geophysical Research: Space Physics*, *123*(6), 4879–4894. https://doi.org/10.1029/2017ja024954

Wang, C., & Branduardi-Raymond, G. (2018). Progress of solar wind magnetosphere ionosphere link explorer (SMILE) mission. *Chinese Journal of Space Science*, *38*(5), 657–661. https://doi.org/10.11728/cjss2018.05.657

Wang, X., Lu, J., Wang, M., Zhou, Y., & Hao, Y. (2023). Simultaneous observation of magnetopause expansion under radial IMF and indention by HSJ. *Geophysical Research Letters*, *50*(20), e2023GL105270. https://doi.org/10.1029/2023gl105270

Xu, Q., Tang, B., Sun, T., Li, W., Zhang, X., Wei, F., et al. (2022). Modeling of the subsolar magnetopause motion under interplanetary magnetic field southward turning. *Space Weather*, *20*(12), e2022SW003250. https://doi.org/10.1029/2022sw003250